FOCUS ISSUE OF SELECTED PAPERS FROM IMLB 2016 WITH INVITED PAPERS CELEBRATING 25 YEARS OF LITHIUM ION BATTERIES

Li_4SnS_4 and Li_4SnSe_4: Simulations of Their Structure and Electrolyte Properties

Ahmad Al-Qawasmeh, Jason Howard,* and N. A. W. Holzwarth,z**

Department of Physics, Wake Forest University, Winston-Salem, North Carolina 27109-7507, USA

Recent experimental literature reports the solid state electrolyte properties of Li_4SnS_4 and Li_4SnSe_4, identifying interesting questions regarding their structural details and motivating our first principles simulations. Together with Li_4GeS_4, these materials are all characterized by the orthorhombic space group *Pnma* and are found to be isostructural. They have a ground state crystal structure (denoted $Li_4SnS_4^0$) having interstitial sites in void channels along the *c*-axis. They also have a meta-stable structure (denoted $Li_4SnS_4^*$) which is formed by moving one fourth of the Li ions from their central sites to the interstitial positions, resulting in a 0.5 Å contraction of the *a* lattice parameter. Relative to their ground states, the meta-stable structures are found to have energies 0.25 eV, 0.02 eV, and 0.07 eV for $Li_4GeS_4^*$, $Li_4SnS_4^*$, and $Li_4SnSe_4^*$, respectively. Consistent with these simulation results, the ground state forms for $Li_4GeS_4^0$, $Li_4SnS_4^0$ and $Li_4SnSe_4^0$ and the meta-stable form for $Li_4SnS_4^*$ have been reported in the experimental literature. In addition, simulations of Li ion migration in these materials are also investigated.

Manuscript submitted September 29, 2016; revised manuscript received November 8, 2016. Published January 18, 2017. This was Paper 842 presented at the Chicago, Illinois, Meeting of the IMLB, June 19–24, 2016. *This paper is part of the Focus Issue of Selected Papers from IMLB 2016 with Invited Papers Celebrating 25 Years of Lithium Ion Batteries.*

Recently, there has been significant progress in developing stable solid electrolytes with high ionic conductivity,[1] which has been identified as a key to improving battery technologies.[2] Recent literature[3–7] reports the use of Li_4SnS_4 and related materials as relatively stable solid electrolytes for use in all-solid-state Li batteries. Kaib, Haddadpour, et al.[3] and Kaib, Bron, et al.[5] synthesized Li_4SnS_4 and Li_4SnSe_4, showing that pure materials could be obtained by removing water or methanol from solution based preparations, and comparing their structures and ionic conductivities. MacNeil et al.[4] used high temperature solid state techniques to synthesize Li_4SnS_4 and made a detailed structural analysis to show it to be isostructural with Li_4GeS_4. Sahu et al.[6] showed that Li_4SnS_4 and its alloys with Li_3AsS_4 have reasonable ionic conductivity (10^{-5}–10^{-4} S/cm at room temperature) with comparatively more air-stability than other sulfide electrolytes. Park et al.[7] demonstrated favorable conductivity and stability properties of Li_4SnS_4 and its alloys with LiI.

From this literature, some interesting questions arise regarding crystal structures and mechanisms for ion mobility. In order to address these questions, we use first principles methods to examine the ideal crystal forms and defect structures of Li_4SnS_4 and the structurally and chemically related materials Li_4GeS_4 and Li_4SnSe_4. For each of these materials, we identify two closely related structures – an ideal ground state structure and an ideal meta-stable structure. The simulations show that the meta-stable structural form is most accessible to Li_4SnS_4 of the three materials studied. The simulations are extended to study mechanisms of Li ion migration in both Li_4SnS_4 and Li_4SnSe_4 and are related to the experimental results reported in the literature.

Computational Methods

The computational methods used in this work are based on density functional theory (DFT),[8,9] using the projected augmented wave (PAW)[10] formalism. The PAW basis and projector functions were generated by the ATOMPAW[11] code and the crystalline materials were modeled using the QUANTUM ESPRESSO[12] and ABINIT[13] packages. Visualizations were constructed using the *XCrySDEN*,[14,15] and *VESTA*[16] software packages.

The exchange correlation function is approximated using the local-density approximation (LDA).[17] The choice of LDA functional was made based on previous investigations[18–20] of similar materials which showed that, provided that the lattice constants are scaled by a correction factor of 1.02, the simulations are in good agreement with experiment, especially lattice vibrational frequencies and heats of formation. The partial densities of states were calculated as described in previous work,[20,21] using weighting factors based on the charge within the augmentation spheres of each atom with radii $r_c^{\rm Li} = 1.6$, $r_c^{\rm Sn} = 2.3$, $r_c^{S} = 1.7$, and $r_c^{\rm Se} = 2.3$ in bohr units. The reported partial densities of states curves $< N^a(E) >$ were averaged over the atomic sites of each type *a*.

The calculations were well converged with plane wave expansions of the wave function including $|\mathbf{k}+\mathbf{G}|^2 \leq 64$ bohr^{-2}. Calculations for the conventional unit cells were performed using a Brillouin-zone sampling grid of $4 \times 8 \times 8$. Simulations of Li ion migration were performed at constant volume in supercells constructed from the optimized conventional cells extended by $1 \times 2 \times 2$ and a Brillouin-zone sampling grid of $2 \times 2 \times 2$. In modeling charged defects (Li ion vacancies or interstitials), the system was assumed to remain electrically insulating and a uniform background charge was added in order to evaluate the electrostatic interactions. The minimum energy path for Li ion migration was estimated using the "nudged elastic band" (NEB) method[22–24] as programmed in the QUANTUM ESPRESSO package, using 5 images between each metastable configuration. For each minimum energy path, the migration energy, E_m was determined as the energy difference between the lowest and highest energy of the path. The "formation energies" E_f for producing neutral defects in the form of vacancy-interstitial pairs were calculated for the same supercells. The molecular dynamics simulations were performed at constant volume in neutral $1 \times 2 \times 2$ supercells using further reduced convergence parameters, including a reduced plane wave expansion cutoff of $|\mathbf{k}+\mathbf{G}|^2 \leq 49$ bohr^{-2} and a Brillouin-zone sampling grid of $1 \times 1 \times 1$. The simulations were performed for a microcanonical ensemble with a time integration step of $\Delta t = 3.6 \times 10^{-15}$ s for simulation temperatures less than 900 K. For simulation temperatures greater than 900 K, the time integration step was reduced to $\Delta t = 2.4 \times 10^{-15}$ s. This resulted in total energy conservation within 0.1 eV throughout the simulation. The simulations were carried out for durations between 3-8 pico seconds. After an equilibration delay of approximately 0.1 ps, the temperature of the simulation was determined from the averaged kinetic energy of the ions. The

*Electrochemical Society Student Member.
**Electrochemical Society Member.
zE-mail: natalie@wfu.edu

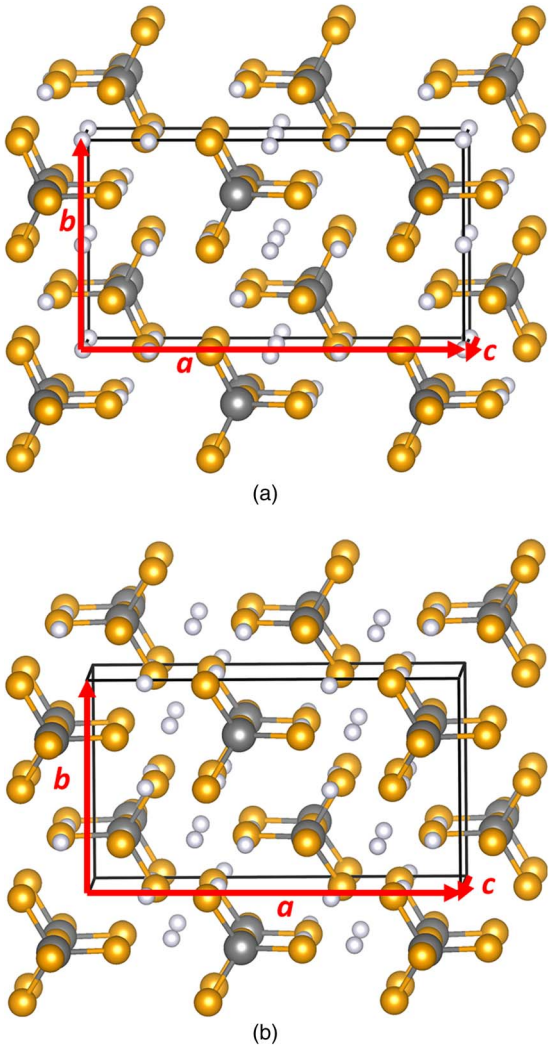

Figure 1. Ball and stick models of (a) $Li_4SnS_4^0$ and (b) $Li_4SnS_4^*$. Li, Sn, and S are represented by light gray, dark gray, and orange balls respectively. The red arrows indicate the *a*, *b*, and *c* lattice vectors.

simulated temperatures ranged between 550 K and 1000 K, well below the melting temperature of 1231 K reported by MacNeil et al.[4]

Simulated Crystal Structures

There are two reported analyses of the crystal structure of Li_4SnS_4.[3,4] The two analyses agree that the structure is characterized by the space group *Pnma* (No. 62 in the International Table of Crystallography[25]), but differ slightly in the reported lattice constants and the fractional coordinates of one of the Li sites.[4] The structural analysis of MacNeil et al.[4] was measured at room temperature and is perfectly ordered. However, the structural analysis of Kaib, Haddadpour, et al.,[3] was measured at the temperatures in the range 100–193 K, and instead of the Li sites found by MacNeil et al. at the Wyckoff labeled 4*a* positions, fractionally occupied 8*d* Li sites are found.

We computationally investigated both structures, finding that the ordered structure analyzed by MacNeil et al.[4] to be the ground state structure which we denote as "$Li_4SnS_4^0$". Simulations of ordered approximations to the disordered structure of Kaib, Haddadpour, et al.[3] find a meta-stable structure which we denote as "$Li_4SnS_4^*$" having an energy 0.02 eV/formula unit higher in energy than the ground state structure. Ball and stick drawings of the two structures are shown in Fig. 1. The corresponding calculated and measured lattice constants are listed in Table I and the calculated and measured fractional coordinates are listed in Table II. In addition to results for Li_4SnS_4, results for Li_4GeS_4 and Li_4SnSe_4 are also listed in these tables.

Table I. Comparison of lattice parameters for Li_4SnS_4 and related compounds in their ground state and meta-stable structures. Calculated parameters are scaled by factor of 1.02 to correct for systematic LDA error. Measured parameters are listed in parentheses. The relative energies *E* for the ground state and meta-stable structures are also listed in units of eV per formula unit.

	$Li_4GeS_4^0$	$Li_4GeS_4^*$
a (Å)	14.01 (14.06)[a]	13.49
b (Å)	7.74 (7.75)[a]	7.79
c (Å)	6.12 (6.15)[a]	6.30
E (eV/FU)	0.00	0.25
	$Li_4SnS_4^0$	$Li_4SnS_4^*$
a (Å)	14.25 (14.31)[a]	13.81 (13.81)[b]
b (Å)	7.86 (7.90)[a]	7.93 (7.96)[b]
c (Å)	6.31 (6.33)[a]	6.41 (6.37)[b]
E (eV/FU)	0.00	0.02
	$Li_4SnSe_4^0$	$Li_4SnSe_4^*$
a (Å)	14.98 (14.93)[c]	14.48
b (Å)	8.26 (8.22)[c]	8.38
c (Å)	6.62 (6.60)[c]	6.86
E (eV/FU)	0.00	0.07

[a]Ref. 4.
[b]Ref. 3.
[c]Ref. 5.

Interestingly, the main difference between the simulated structures of $Li_4SnS_4^0$ and $Li_4SnS_4^*$ is that four Li's per unit cell occupy different void regions between the SnS_4 tetrahedra. In the $Li_4SnS_4^0$ structure, the special Li ions occupy sites at the center and boundaries of the unit cell having multiplicity and Wyckoff label 4*a*. In the $Li_4SnS_4^*$ structure, the special Li ions instead occupy sites interior to the unit cell having multiplicity and Wyckoff label 4*c*. In order to avoid confusion of this site with the other fully occupied 4*c* Li site of these structures, we use the symbol *c*′ to refer to this site. While the simulated fractional coordinates of the special Li ions for this 4*c*′ site do not agree with the two 8*d* fractionally occupied coordinates found by Kaib, Haddadpour, et al.,[3] the optimized lattice constants are in excellent agreement, as shown in Table I. It is interesting to note that the lattice constants for these ideal structures are characterized by a contraction of the *a* lattice parameter by approximately 0.5 Å for the meta-stable structure relative to the ground state structure, while the changes to the other lattice parameters are in the neighborhood of 0.1 Å. This lattice contraction is energetically significant; the energy difference between $Li_4SnS_4^*$ calculated with the lattice constants of $Li_4SnS_4^0$ relative to Li_4SnS_4 calculated with its optimized lattice constants is 0.03 eV/formula unit. We should also point out that the original X-ray analysis of Kaib, Haddadpour, et al.,[3] for the $Li_4SnS_4^*$ structure was performed at low temperatures (100–193 K) while the X-ray analysis of MacNeil et al.[4] was performed at room temperature. It is our experience that lattice constants typically change with temperature by less than 0.1 Å, so that the lattice constant differences between the $Li_4SnS_4^0$ and $Li_4SnS_4^*$ structures should not be attributed to temperature alone. In addition, Sahu et al.[6] report room temperature X-ray analysis for $Li_4SnS_4^*$ consistent with an expansion of the lattice by approximately 0.02 Å.

Because of its low atomic number, the X-ray signal for Li positions is notoriously small so that it is reasonable to ask whether the simulated $Li_4SnS_4^*$ structure might be compatible with the structural data reported by Kaib, Haddadpour, et al.,[3] even if the site analysis differs. Using the Mercury software package,[26] with the structural data from experiment and simulations we compare the computed X-ray patterns for the structures of $Li_4SnS_4^0$ and $Li_4SnS_4^*$ in Fig. 2. We see that the patterns for $Li_4SnS_4^0$ and $Li_4SnS_4^*$ are distinguishable and that there

Table II. Comparison of fractional coordinates of unique atomic positions for Li_4SnS_4 and related compounds in their ground state and meta-stable structures, using orientation and origin choice given in Ref. 4. The second column lists the site multiplicity and Wyckoff label. We use the notation c' to denote the special Li site which characterizes the meta-stable structures. Measured parameters are listed in square brackets when available.

Atom	Site	$Li_4GeS_4^0$ (x, y, z)	$Li_4GeS_4^*$ (x, y, z)
Li	4*a*	(0.000, 0.000, 0.000) [(0.000, 0.000, 0.000)][a]	–
Li	4*c*′	–	(0.260, 0.250,-0.001)
Li	4*c*	(0.412, 0.250, 0.127) [(0.412, 0.250, 0.129)][a]	(0.429, 0.250, 0.216)
Li	8*d*	(0.177, 0.000, 0.186) [(0.178, 0.000, 0.192)][a]	(0.147,-0.023, 0.139)
Ge	4*c*	(0.089, 0.250, 0.645) [(0.089, 0.250, 0.649)][a]	(0.097, 0.250, 0.620)
S	4*c*	(0.084, 0.250, 0.277) [(0.086, 0.250, 0.291)][a]	(0.105, 0.250, 0.261)
S	8*d*	(0.158, 0.010, 0.780) [(0.157, 0.015, 0.779)][a]	(0.177, 0.019, 0.761)
S	4*c*	(0.437, 0.250, 0.728) [(0.439, 0.250, 0.731)][a]	(0.434, 0.250, 0.810)
Atom	Site	$Li_4SnS_4^0$ (x, y, z)	$Li_4SnS_4^*$ (x, y, z)
Li	4*a*	(0.000, 0.000, 0.000) [(0.000, 0.000, 0.000)][a]	–
Li	4*c*′	–	(0.287, 0.250. 0.003) [-][b]
Li	4*c*	(0.410, 0.250, 0.124) [(0.409, 0.250, 0.126)][a]	(0.429, 0.250, 0.359) [(0.430, 250, 0.338)][b]
Li	8*d*	(0.176, 0.003, 0.178) [(0.178, 0.004, 0.179)][a]	(0.158,-0.004, 0.149)[(0.160, 0.005, 0.154)][b]
Sn	4*c*	(0.093, 0.250, 0.640) [(0.092, 0.250, 0.642)][a]	(0.090, 0.250, 0.633) [(0.087, 0.250, 0.635)][b]
S	4*c*	(0.080, 0.250, 0.255) [(0.083, 0.250, 0.267)][a]	(0.092, 0.250, 0.256) [(0.091, 0.250, 0.263)][b]
S	8*d*	(0.152,-0.005, 0.787) [(0.161, 0.001, 0.784)][a]	(0.158,-0.004, 0.149) [(0.167, 0.007, 0.767)][b]
S	4*c*	(0.430, 0.250, 0.732) [(0.432, 0.250, 0.766)][a]	(0.423, 0.250, 0.748) [(0.424, 0.250, 0.736)][b]
Atom	Site	$Li_4SnSe_4^0$ (x, y, z)	$Li_4SnSe_4^*$ (x, y, z)
Li	4*a*	(0.000, 0.000, 0.000) [(0.000, 0.000, 0.000)][c]	–
Li	4*c*′	–	(0.282, 0.250, 0.002)
Li	4*c*	(0.413, 0.250, 0.118) [(0.412, 0.250, 0.106)][c]	(0.428, 0.250, 0.358)
Li	8*d*	(0.175, 0.003, 0.178) [(0.178, 0.005, 0.180)][c]	(0.157, -0.006, 0.147)
Sn	4*c*	(0.094, 0.250, 0.639) [(0.092, 0.250, 0.643)][c]	(0.090, 0.250, 0.630)
Se	4*c*	(0.080, 0.250, 0.252) [(0.082, 0.250, 0.264)][c]	(0.093, 0.250, 0.250)
Se	8*d*	(0.162,-0.008, 0.785) [(0.161,-0.002, 0.784)][c]	(0.177, 0.005, 0.770)
Se	4*c*	(0.430, 0.250, 0.725) [(0.432, 0.250, 0.728)][c]	(0.422, 0.250, 0.750)

[a]Ref. 4.
[b]Ref. 3, omitting fractionally occupied Li position.
[c]Ref. 5.

seems to be good agreement between our simulated structures and the corresponding X-ray results. While it would be better to compare the simulated diffraction patterns directly with the experimental data, the good agreement between the simulations and the fitted results from experiment shown in Fig. 2 is encouraging. It is interesting to note that two other groups[6,7] have recently reported preparations of Li_4SnS_4 using relatively low temperature processing similar to that of Kaib, Haddadpour, et al.[3] Both of these studies report X-ray diffraction patterns, presumably measured at room temperature, which show strong similarity to the patterns for $Li_4SnS_4^*$ shown in Fig. 2. Presumably, the ground state $Li_4SnS_4^0$ structure is accessible using the higher temperature processes described by MacNeil et al.[4]

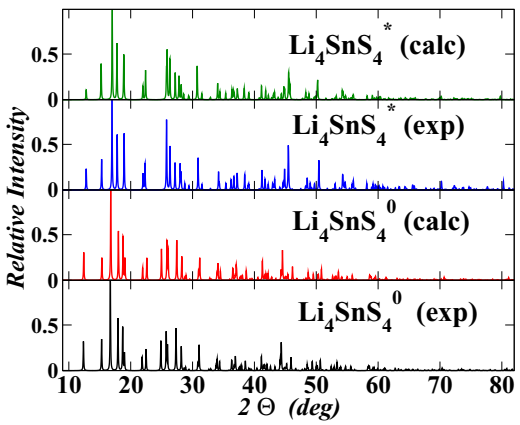

Figure 2. X-ray diffraction patterns generated by the Mercury software package[26] assuming an X-ray wavelength of $\lambda = 1.54056$ Å, comparing simulation (calc) and experimental (exp) results for the $Li_4SnS_4^0$ and $Li_4SnS_4^*$ structures. The structural parameters from experiment were taken from Ref. 4 for $Li_4SnS_4^0$ and from Ref. 3 for $Li_4SnS_4^*$.

It is interesting to ask the question whether the structurally and chemically similar material Li_4GeS_4 behaves in a similar way. The simulation results for the the $Li_4GeS_4^0$ and $Li_4GeS_4^*$ structures are listed in Table I and in Table II together with available experimental values. The fractional coordinates are very similar to those of Li_4SnS_4. However, in this case, we would predict that the meta-stable $Li_4GeS_4^*$ structure is less likely to form since its energy is predicted to be 0.25 eV/formula unit higher in energy than the ground state energy. The investigation was also extended to Li_4SnSe_4 which was recently synthesized by Kaib, Bron, et al.[5] using relatively high temperature techniques. These authors find Li_4SnSe_4 to take the "ground state" $Li_4SnSe_4^0$ structure. Our simulations find that the meta-stable $Li_4SnSe_4^*$ to have an energy of 0.07 eV/formula unit higher in energy than the ground state structure, suggesting that it is less likely than $Li_4SnS_4^*$ to form at room temperature. The results are listed in Table I and in Table II.

Electronic Structure Results

In order to gain a qualitative understanding of the electronic structure of the various forms of of these materials, it is helpful to analyze the partial densities of states which are shown in Fig. 3. The partial density of states of $Li_4GeS_4^0$ in its ground state structure was previously presented in Ref. 27. While, density functional theory is known to systematically underestimate the band gaps, the relative band gaps are usually well represented. For these materials, Li_4GeS_4 has a computed bandgap of 2.1 eV, while the computed band gaps for Li_4SnS_4 and Li_4SnSe_4 are 2.2 eV and 1.6 eV respectively. For both of these

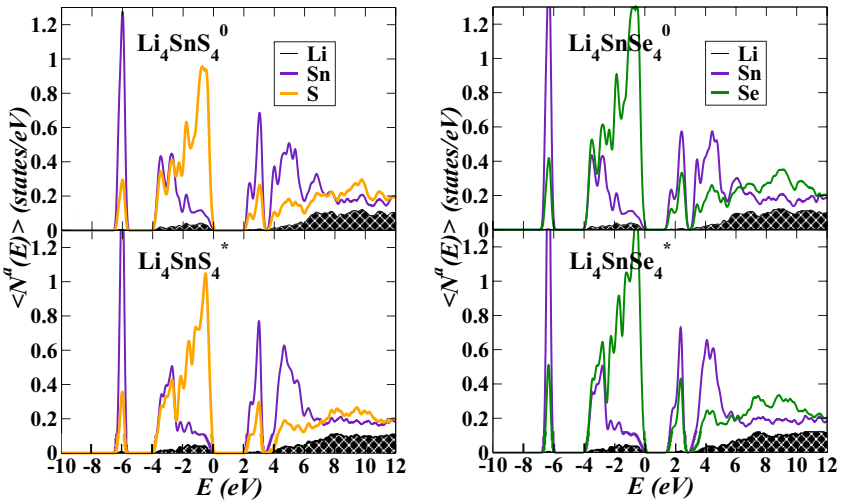

Figure 3. Partial densities of states for $Li_4SnS_4^0$ and $Li_4SnS_4^*$ (a) and $Li_4SnSe_4^0$ and $Li_4SnSe_4^*$ (b), separately indicating contributions from Li, Sn, S, and Se sites.

materials the upper part of the valence band is dominated by chalcogenide states while the conduction band is dominated by Sn 5*s* states forming a narrow band below the Sn 5*p* states. The results for Li_4SnS_4 presented in Fig. 3 are consistent with the results previously reported by MacNeil et al.[4] The partial densities of states for the ground state and meta-stable structures have nearly indistinguishable partial density of states curves. The materials are clearly insulating with band gaps expected to be larger than 2 eV found in the present study due to the systematic gap underestimation known for LDA calculations.

Another result from the electronic structure calculations is the total energies which approximate the internal energies at zero temperature. These can be used to study the stability of the materials relative to various possible reactions such as those listed in Table III. If the effects of zero point motion and finite temperature are small, the results can be related to experimental enthalpies. The values listed in this table correspond to the ground state structures of $Li_4SnCh_4^0$. Results for the meta-stable form of $Li_4SnCh_4^*$ can be determined by adding 0.02 eV or 0.07 eV for Ch=S or Ch=Se, respectively. Reaction 1 listed in Table III corresponds the enthalpy of formation referenced to the standard states of the elements[28] including Li in the bcc structure, Sn in the diamond structure, S in the orthorhombic structure,[29] and Se in the trigonal structure.[30] Reaction 2 listed in Table III corresponds to decomposition into two binary materials. Li_2S and Li_2Se both form in the fluorite structure, while SnS_2 and $SnSe_2$ both form in the hexagonal CdI_2 structure. Our simulations indicate that the two reactions have opposite sign, meaning that Li_4SnS_4 is more stable than its binary products, while Li_4SnSe_4 is less stable. Reaction 3 listed in Table III involves two new materials with the stoichiometry Li_2SnCh_3. Recently, Brant et al.[31] synthesized and characterized Li_2SnS_3, finding it to have a densely packed layered structure. The electronic structure results indicate that Li_2SnS_3 together with excess Li_2S is more stable than Li_4SnS_4. Li_2SnSe_3 was recently synthesized by Kaib, Bron, et al.[5], characterized by one dimensional chains of SnS_4 tetrahedra. The electronic structure results indicate that this material together with excess Li_2Se has about the same stability as Li_4SnSe_4.

Table III. Estimates of various reaction energies (in eV) for Li_4SnCh_4 for the calcogens Ch=S and Ch=Se based on total energy calculations. In each case the ground state structures of $Li_4SnCh_4^0$ was assumed; the structures of the products are mentioned in the text of the manuscript.

	Reaction	Ch=S	Ch=Se
1	$Li_4SnCh_4 \rightarrow 4Li + Sn + 4Ch$	−9.99	−8.94
2	$Li_4SnCh_4 \rightarrow 2Li_2Ch + SnCh_2$	−0.09	0.04
3	$Li_4SnCh_4 \rightarrow Li_2Ch + Li_2SnCh_3$	0.17	−0.01

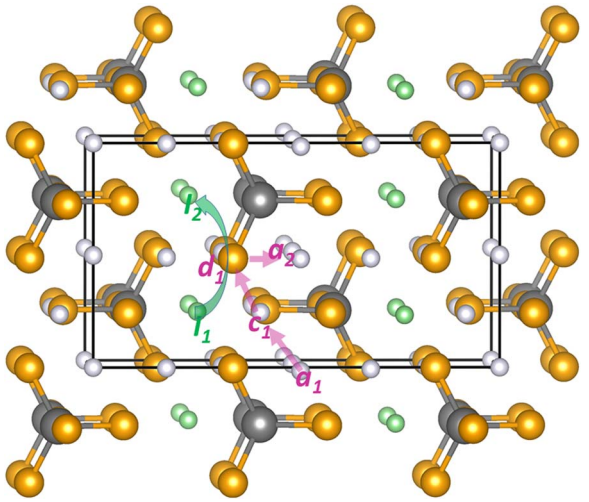

Figure 4. Ball and stick model of ground state structure of $Li_4SnS_4^0$ and $Li_4SnSe_4^0$ using the same ball convention and viewpoint as in Fig. 1(a). Distinct vacancy sites are indicated with their Wyckoff labels a_i, c_i, and d_i. Interstitial sites are colored green and are labeled I_i. Possible vacancy and interstitialcy trajectories are indicated with transparent purple and green arrows respectively.

Defect Structures and Ion Migration Paths in $Li_4SnS_4^0$, $Li_4SnS_4^*$, $Li_4SnSe_4^0$, and $Li_4SnSe_4^*$.

Point defects were modeled at fixed volume in $1 \times 2 \times 2$ supercells. For the ground state structure of $Li_4SnS_4^0$ and $Li_4SnSe_4^0$, there are three distinct Li ion vacancy sites which can be uniquely labeled by the Wyckoff letters a_i, c_i, and d_i as visualized in Fig. 4. The vacancy energies are listed in Table IV relative to the most stable vacancy at an *a* site.

Vacancy migration in $Li_4SnSe_4^0$ was previously studied by Kaib, Bron, et al.[5] who showed that a sequence of hops of the vacancy between the sites $a_1 \rightarrow c_1 \rightarrow d_1 \rightarrow a_2 \ldots$ results in net ion motion

Table IV. Relative energies (in eV) of vacancies in the ground state structures of $Li_4SnS_4^0$ and $Li_4SnSe_4^0$ calculated in 1 × 2 × 2 supercells. The vacancy sites are indicated by their Wyckoff site labels with the zero energy chosen at the *a* site.

Vacancy label	$Li_4SnS_4^0$	$Li_4SnSe_4^0$
a	0.00	0.00
c	0.30	0.20
d	0.26	0.16

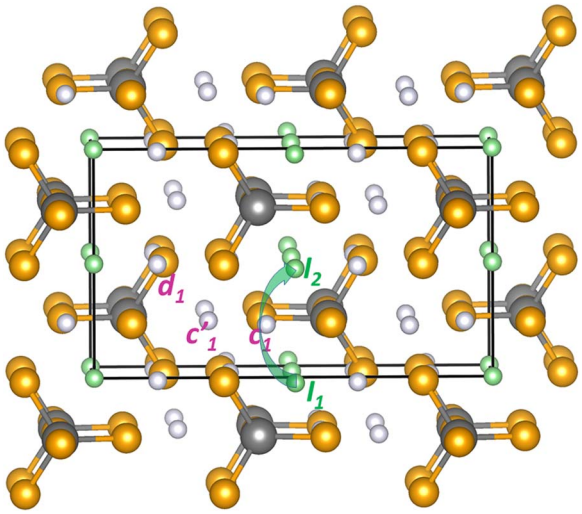

Figure 5. Ball and stick model of ground state structure of $Li_4SnS_4^*$ and $Li_4SnSe_4^*$ using the same ball convention and viewpoint as in Fig. 1(b). Distinct vacancy sites are indicated with their Wyckoff labels c'_i, c_i, and d_i. Interstitial sites are colored green and are labeled I_i. Possible interstitialcy trajectories are indicated with transparent green arrows.

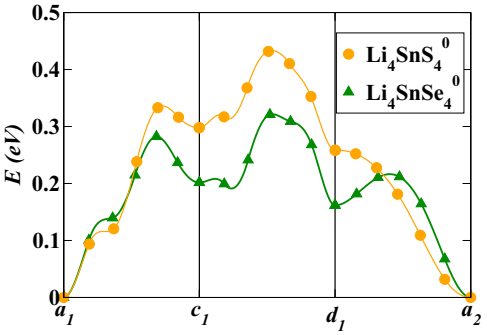

Figure 6. NEB calculated energy path diagram for Li ion vacancy migration in $Li_4SnS_4^0$ and $Li_4SnSe_4^0$. The vacancy site labels correspond to the diagram in Fig. 4.

in the b and c directions in the crystal as illustrated in Fig. 4. The corresponding energies along this path as calculated using the NEB method are shown in Fig. 6 and tabulated in Table V. From Table V we see that the vacancy hopping distances d are slightly smaller and the path energies are somewhat larger for $Li_4SnS_4^0$ compared with $Li_4SnSe_4^0$. The bottleneck of this process occurs during the $c_1 \rightarrow d_1$ step, resulting in the estimated migration energies of $E_m = 0.46$ eV and $E_m = 0.32$ eV for $Li_4SnS_4^0$ and $Li_4SnSe_4^0$, respectively. Another vacancy migration path for this involves vacancy hopping between the sites $a \rightarrow c \rightarrow a \rightarrow c \ldots$ resulting in net migration along the b axis. The estimated migration energy for this path is $E_m = 0.33$ eV and $E_m = 0.28$ eV for $Li_4SnS_4^0$ and $Li_4SnSe_4^0$, respectively. We also investigated vacancy migration mechanisms along the a axis. The bottleneck for a axis vacancy migration involves hops between

Table V. NEB calculated migration energies (E_m) and ideal distances (d) for vacancy migration in $Li_4SnS_4^0$ and $Li_4SnSe_4^0$. Migration energies are referenced to a vacancy at the a site.

	$Li_4SnS_4^0$		$Li_4SnSe_4^0$	
	E_m (eV)	d (Å)	E_m (eV)	d (Å)
$a \rightarrow c$	0.33	3.3	0.28	3.5
$c \rightarrow d$	0.46	3.6	0.32	3.8
$d \rightarrow a$	0.26	2.8	0.21	2.9

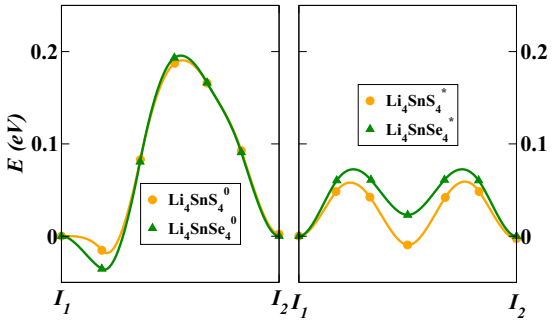

Figure 7. NEB calculated energy path diagram for Li ion migration with an interstitialcy mechanism as shown in Fig. 4 for $Li_4SnS_4^0$ and $Li_4SnSe_4^0$ and as shown in Fig. 5 for $Li_4SnS_4^*$ and $Li_4SnSe_4^*$.

nearest neighbor d sites which raise the estimated migration energies substantially above the migration barriers along the b and c axes. In general there is good agreement between our calculated results for $Li_4SnSe_4^0$ and the corresponding results of Kaib, Bron, et al.,[5] within a small descrepancy of 0.03 eV or less.

For the meta-stable structure of $Li_4SnS_4^*$, only the c' site vacancy is stable. Calculations initialized with vacancies on c or d sites relax to a vacancy on nearby c' site. For the meta-stable structure of $Li_4SnSe_4^*$, the story is slightly different. For that system, the c' site vacancy is again the most stable. Calculations initialized with vacancies on a c site relax to a vacancy on a nearby c' site. Calculations initialized with vacancies on a d site are meta-stable with considerable distortion, having an energy of 0.24 eV above the energy of the c' site vacancy. We did not investigate vacancy migration mechanisms in the meta-stable structures.

Another important mechanism for ion migration involves interstitial sites. For the ground state structures of $Li_4SnS_4^0$ and $Li_4SnSe_4^0$ there is one main interstitial site located in the void regions between SnS_4 or $SnSe_4$ tetrahedra as shown in Fig. 4 which happens to be the c' Li site of the meta-stable $Li_4SnS_4^*$ and $Li_4SnSe_4^*$ structures. Correspondingly, for the meta-stable structures of $Li_4SnS_4^*$ and $Li_4SnSe_4^*$ the one main interstitial site is located in the void regions which happens to be the a site of the ground state structures as shown in Fig. 5. For both structures, migration between these interstitial sites occurs most efficiently using an "interstitialcy" mechanism. An interstitialcy mechanism is one in which an interstitial ion moves into a host lattice site as that host lattice ion moves to an adjacent interstitial site. The resulting migration processes for $Li_4SnS_4^0$ and $Li_4SnSe_4^0$, with an intermediate d host lattice site, and for $Li_4SnS_4^*$ and $Li_4SnSe_4^*$, with an intermediate c host lattice site, are illustrated with the green arrows in Figs. 4 and 5 and the corresponding NEB energy paths are shown in Fig. 7.

From the energy path diagram shown in Fig. 7, it is evident that the interstitialcy mechanism results in the lowest migration barrier for all of the structures investigated and is predicted to dominate migration processes. For electrolytes in the so-called "intrinsic" regime, the NEB estimate of the activation energy E_A^{NEB} for conductivity is related to the migration energy E_m and the formation energy E_f to form a vacancy and interstitial pair according to

$$E_A^{\mathrm{NEB}} = E_m + \frac{1}{2}E_f. \qquad [1]$$

A summary of results including optimal calculated values of E_A^{NEB} from Eq. 1 and available experimental values are listed in Table VI. For the ground state structures of $Li_4SnS_4^0$ and $Li_4SnSe_4^0$ the calculated optimal values of E_f were obtained for vacancies on an a site moving to the nearest interstitial site Ic' which corresponds to the site we've called c' in the meta-stable structures. The calculated values of E_f are 0.27 eV and 0.36 eV for $Li_4SnS_4^0$ and $Li_4SnSe_4^0$, respectively. The corresponding estimates of the activation energies E_A^{NEB} are 0.3 eV and 0.4 eV for $Li_4SnS_4^0$ and $Li_4SnSe_4^0$, respectively. To the best of our

Table VI. Activation energies for ion migration for ground state and meta-stable state structures of Li_4SnS_4 and Li_4SnSe_4. Calculated migration energies E_m were determined from NEB calculations of the interstitialcy mechanism shown in Fig. 7. Formation energies E_f for interstitial-vacancy pairs, calculated activation energies E_A^{NEB} based on Eq. 1 and literature values of the activation energy E_A^{exp} are also listed. For comparison, the calculated activation energies E_A^{trace} and their error estimates associated with the Arrhenius temperature dependence of the simulated "tracer" diffusion coefficients $D^{trace}(T)$ are also listed here and will be discussed in the Molecular dynamics section.

	E_m (eV)	E_f (eV)	E_A^{NEB} (eV)	E_A^{exp} (eV)	E_A^{trace} (eV)
$Li_4SnS_4^0$	0.19	0.27	0.3		0.24 ± 0.06
$Li_4SnS_4^*$	0.06	0.15	0.1	0.41[a]	0.25 ± 0.04
$Li_4SnSe_4^0$	0.20	0.36	0.4	0.45[b]	0.23 ± 0.1
$Li_4SnSe_4^*$	0.07	0.15	0.1		0.08 ± 0.01

[a]Ref. 3.
[b]Ref. 5.

knowledge, there are no published conductivity measurements for the $Li_4SnS_4^0$ material, but $Li_4SnSe_4^0$ has been well studied by Kaib, Bron, et al.[5] Our NEB calculated result for $Li_4SnSe_4^0$ is in disagreement with the value of 0.6 eV calculated by Kaib, Bron, et al.,[5] but is in better agreement with the value of $E_A = 0.45$ eV deduced from fitting the temperature dependence of the experimental conductivity measurements in the same study.

For the meta-stable structures of $Li_4SnS_4^*$ and $Li_4SnSe_4^*$, the calculated optimal values of E_f were obtained for vacancies on an c' site moving to the nearest interstitial site Ia which corresponds to the a site in the ground state structures. The calculated values of E_f are 0.15 eV for both $Li_4SnS_4^*$ and $Li_4SnSe_4^*$, resulting in estimates of the activation energies E_A^{NEB} of 0.1 eV for both materials. This result is not in agreement with the value of $E_A = 0.41$ eV obtained from fitting the temperature dependence of the experimental conductivity measured by Kaib, Haddadpour, et al.[3]

Molecular Dynamics Simulations

In studying the ion migration mechanisms for the $Li_4SnCh_4^0$ and $Li_4SnCh_4^*$ structures, we find the Li ion motions to be highly correlated presumably due to a complicated energy landscape. For example, in creating single defects in an otherwise perfect lattice, we found some of the configurations to be unstable. For example, in the $Li_4SnS_4^0$ structure, a d site vacancy is unstable relative to a vacancy on the nearest a site Li. In the $Li_4SnS_4^*$ structure a d site vacancy is unstable relative to a vacancy on the nearest c' site Li. The NEB analysis discussed in the previous section was unable to completely explain the conductivity results. In order to get additional information about the migration processes, we performed molecular dynamics simulations using the QUANTUM ESPRESSO[12] code. While the NEB method gives insight about the probability of individual hops of the migrating Li ions, molecular dynamics simulations provide information about the motions of the ensemble of ions within the simulation cell. As shown by Mo, Ong, and others,[32–35] one way to improve the configuration sampling of the simulations is to perform the simulations at elevated temperatures. The expectation (although unproven) is that the behaviors of the materials at room temperature can be estimated from the extrapolated simulation results.

Figure 8 shows a visualization of the Li mobility with a ball and stick model of the crystals with superposed Li positions at 136 time steps at intervals of 0.05 ps. It is apparent from these diagrams that at the relatively low simulation temperatures of $T = 635$ K and $T = 656$ K there is substantial motion of all of the Li ions. In addition to the vacancy and interstitialcy mechanisms studied by the NEB analysis as discussed above, several other pathways for Li ion motion are evident.

In order to better analyze the molecular dynamics simulations, it is convenient to define a site occupancy factor as a function of time $s_i(t)$ where i denotes the site type. For the ground state structure, the sites were labeled according to their host site type (a, c, or d) or the interstitial site type (Ic'). For the meta-stable state structure, the sites were labeled according to their host site type (c', c, or d) or the interstitial site type (Ia). The site label i was determined from the closest Li position of the perfect lattice relative to the instantaneous position of each Li. For convenience, the site occupancy factors were normalized to unity at full occupancy and followed the sum rule:

$$\sum_i s_i(t)\frac{n_i}{N} = 1, \qquad [2]$$

where n_i denotes the multiplicity of the site and N denotes the total number of Li sites. For the materials in this study, $n_d/N = 2n_j/N$, where j indexes the a, c, or c′ sites and d denotes the d site type. As shown in Fig. 9, the instantaneous site occupancy factors $s_i(t)$ are very noisy and it is convenient to define a time averaged site occupancy parameter

$$\langle s_i \rangle_t \equiv \frac{1}{t}\int_0^t s_i(t')dt'. \qquad [3]$$

As shown in Fig. 9, $\langle s_i \rangle_t$ tends to an asymptotic value at long times.

It is interesting to study the asymptotic time averaged site occupancy factors $\langle s_i \rangle_{t\to\infty} \equiv \langle s_i \rangle$ as a function of simulation temperatures for the four materials as shown in Fig. 10. These values were determined from the final time step of each simulation which was between 3 and 8 ps. The values of $\langle s_i \rangle$ for $Li_4SnS_4^0$ and $Li_4SnSe_4^0$ structures show relative small values (<0.5) for the interstitial Ic' site and relative large values (>0.75) for the host lattice sites (a, c, and d), indicating a relatively well-ordered structure. On the other hand for the $Li_4SnS_4^*$ and $Li_4SnSe_4^*$ structures, the interstitial sites (Ia) are substantially occupied (>0.5) throughout the temperature range, indicating relatively disordered structures.

It is possible to use molecular dynamics results in a more quantitative analysis of ionic conductivity following the approach implemented by Mo, Ong, and others.[32–35] For a molecular dynamics simulation at temperature T with resultant ion trajectories $\{\mathbf{r}_i(t)\}$ as a function of time t, one can calculate the mean squared displacement and use Einstein's expression to determine the diffusion constant $D_{\text{trace}}(T)$:[36]

$$\left\langle \frac{1}{6N}\sum_{i=1}^{N} |\mathbf{r}_i(t) - \mathbf{r}_i(t_0)|^2 \right\rangle = D_{\text{trace}}(T)[t - t_0] + C. \qquad [4]$$

Here the summation over i denotes the N Li ion positions $\{\mathbf{r}_i(t)\}$ in the simulation cell and C denotes a constant. In order to improve the sampling of the simulation, the incremental distance is averaged over the initial times t_0 as implied by the angular brackets in the expression. As pointed out by Murch,[37–39] the temperature dependent diffusion constant $D_{\text{trace}}(T)$ calculated from the mean squared displacement in this way approximates the diffusion of tracked particles such that can experimentally realized in radioactive tracer experiments. Since diffusion takes place near equilibrium, it is reasonable to also assume that the diffusion coefficient has an Arrhenius temperature dependence[40]

$$D_{\text{trace}}(T) = D_{\text{trace}}(0)e^{-E_A^{\text{trace}}/kT}, \qquad [5]$$

where $D_{\text{trace}}(0)$ denotes the diffusion coefficient at 0 K, E_A^{trace} denotes the activation energy for diffusion, and k denotes the Boltzmann constant.

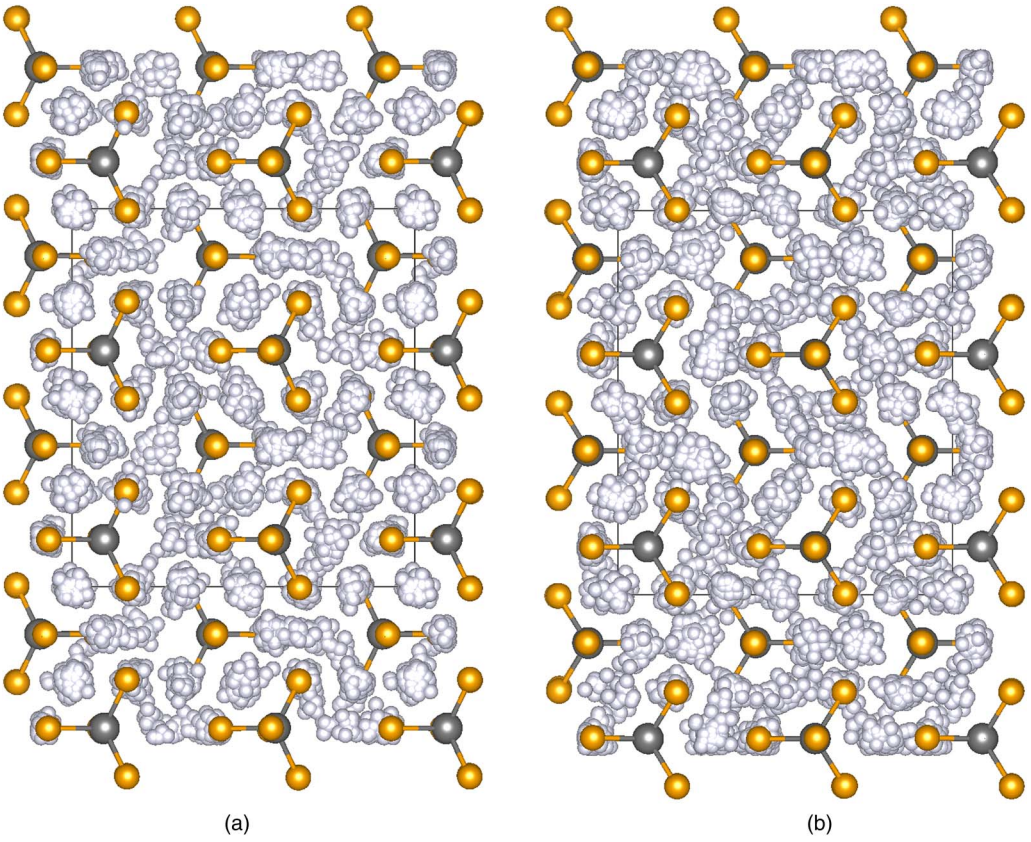

Figure 8. Ball and stick diagrams of molecular dynamics simulations for $Li_4SnS_4^0$ at $T = 635$ K (a) and $Li_4SnS_4^*$ at $T = 656$ K (b). Initial Sn and S positions are represented by gray and orange balls respectively. Li positions of the initial configuration and 136 subesquent positions at time intervals of 0.05 ps are indicated with gray balls. Simulations were performed using microcanonical ensembles (constant energy and volume) in $1 \times 2 \times 2$ supercells. The viewpoint is a projection down the *c*-axis.

The temperature dependent direct-current ionic conductivity is related to $D_{\text{trace}}(T)$ by the equation[38]

$$\sigma(T) = \frac{\rho q^2}{kT} \frac{D_{\text{trace}}(T)}{H}, \qquad [6]$$

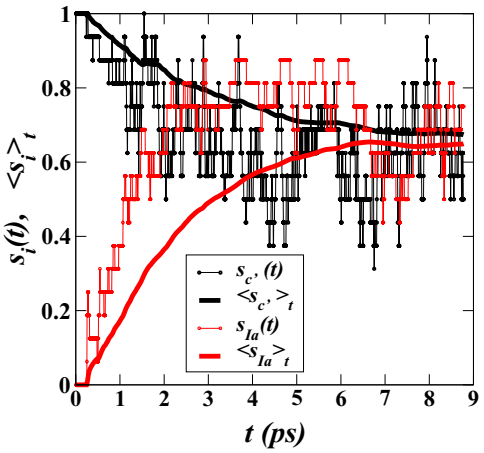

Figure 9. Instantaneous and time averaged site occupancy factors for molecular dynamics simulation of $Li_4SnS_4^*$ at a temperature of $T = 830$ K.

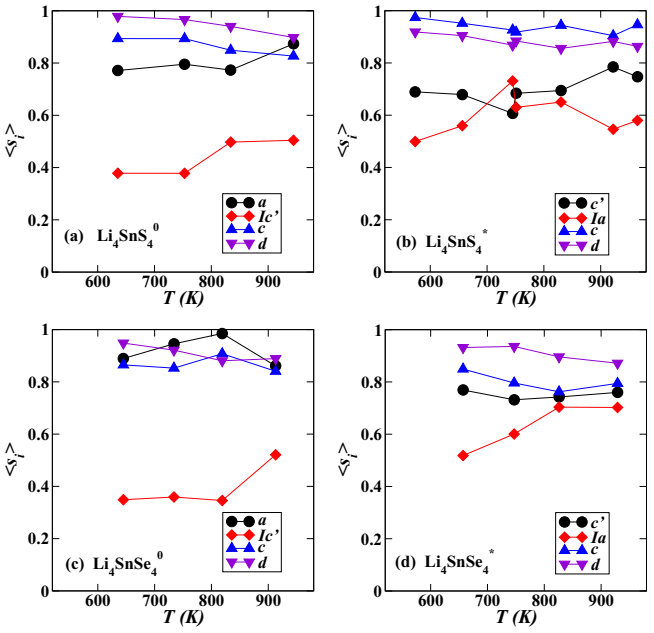

Figure 10. Asymptotic time averaged site occupancy factors $\langle s_i \rangle$ for (a) $Li_4SnS_4^0$, (b) $Li_4SnS_4^*$, (c) $Li_4SnSe_4^0$ and (d) $Li_4SnSe_4^*$ evaluated at various simulation temperatures.

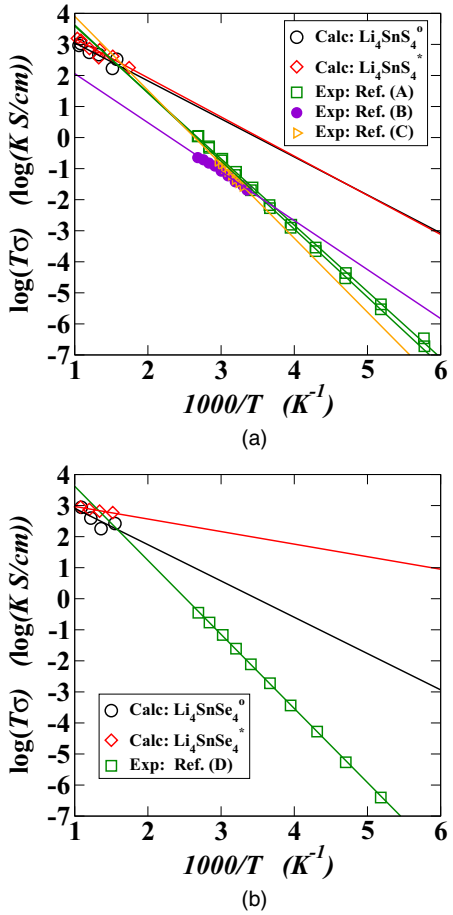

Figure 11. Plots of the ionic conductivity in terms of $\log(T\sigma)$ of Li_4SnS_4 (a) and Li_4SnSe_4 (b). The calculated values were evaluated using Eq. 6 with $H = 1$. The experimental values for $Li_4SnS_4^*$ were taken from Refs. 3 (A), 6 (B), and 7 (C), while experimental results for $Li_4SnSe_4^0$ were taken from Ref. 5 (D). All of the experimental values were analyzed from the published graphs using digitizing software. The lines represent least squares fits to the calculated results or the digitized experimental values.

where ρ denotes the number of mobile ions (Li) per unit volume, q denotes the charge of each Li ion. The factor H is known as the Haven ratio[41] which takes into account so called correlation effects. For example, the conductivity due to an interstitialcy process which involves the concerted motion of interstitial and host ions as discussed above, is not well modeled by the mean squared displacements of independent ions. If the temperature dependence of the Haven ratio H were trivial, the activation energy for tracer diffusion E_A^{trace} would also approximate the activation energy of the conductivity according to Eq. (6). A simulation to estimate the Haven ratio[42] is beyond the scope of the present work. On the other hand, comparing a calculation of the conductivity using Eq. (6) assuming $H = 1$, with experiment, can provide information on the Haven ratios for these materials.

Figure 11 summarizes the simulation results in comparison with experimental conductivity measurements. The conductivity of $Li_4SnS_4^*$ was measured by 3 independent groups,[3,6,7] showing very similar results. The small differences among the experimental conductivity results shown in Fig. 11a may be due to digitization errors. The digitized data from these experiments are consistent with the Arrhenius activation energy of $E_A^{\text{exp}} = 0.4 \pm 0.1$ eV. The simulation results reported here should be regarded as preliminary, due to the relatively small number of configurations sampled. Previous work of this sort[32–35] was based on simulation times 10-100 times as long as our 3-8 ps simulations. For these reasons, the least squares fit lines through the simulated results for $\log(T\sigma)$ versus $1000/T$ should be considered with large error bars.

Mindful of the limitations, it is nevertheless interesting to analyze the simulation results obtained in this study. Despite the differences in their site occupancies, the computed tracer diffusion behaviors of $Li_4SnS_4^0$ and $Li_4SnS_4^*$ shown in Fig. 11a were found to be similar. The magnitudes of the high temperature simulated conductivities is in the range of the extrapolated experimental conductivities. By fitting a straight line through the simulated conductivities, the deduced values of the tracer activation energies are $E_A^{\text{trace}} = 0.24 \pm 0.06$ eV and 0.25 ± 0.04 eV for $Li_4SnS_4^0$ and $Li_4SnS_4^*$ respectively as listed in Table VI. The reported errors of the activation energies are likely underestimates, since they include only errors due to the linear fit and not the additional sampling errors of the simulation. However, these errors suggest that the activation energies for Li ion diffusion in these materials may differ by as much as 0.1 eV. While the tracer diffusion result for $Li_4SnS_4^0$ is consistent with the NEB result, the tracer diffusion result for $Li_4SnS_4^*$ is not in agreement either with experiment or with the NEB estimate for the activation energies. For the selenide materials shown in Fig. 11b, the magnitudes of the high temperature simulated conductivities are again in the range of the extrapolated experimental conductivity. However, in contrast with sulfide materials, the deduced values of the tracer activation energies are distinct; $E_A^{\text{trace}} = 0.23 \pm 0.1$ eV and 0.08 ± 0.01 eV for $Li_4SnSe_4^0$ and $Li_4SnSe_4^*$ respectively as listed in Table VI. The activation energy for tracer diffusion in $Li_4SnSe_4^0$ is smaller than both the values obtained from experimental conductivity measurements and from the NEB calculations. However, the computed E_A^{trace} value for $Li_4SnSe_4^*$ happens to agree well with the NEB estimate of the activation energy E_A^{NEB} which was based on an idealized interstitialcy mechanism. In future work, the molecular dynamics simulations could be improved by reducing the sampling errors in terms of the finite size effects, increasing the simulation times, and considering multiple initial configurations. Additionally, it may be important to go beyond the constant volume simulations and to include the effects of lattice expansion. For example, in the Li_4SnS_4 system, the lattice contraction accounts for an energy gain of 0.03 eV/formula unit. One can guess that the constant volume simulations might bias the systems to result in distinct configurations at high temperature. Perhaps more realistic representations of the volumetric variations with temperature could be used to investigate possible transitions between the structural forms. In addition to these possible numerical improvements, some of the discrepancies of the measured and simulated conductivities come from the Haven ratio which is expected to be non-trivial for these materials due to the importance of the interstitialcy mechanism.

Conclusions

Our simulations identify ideal ground state structures for $Li_4GeS_4^0$, $Li_4SnS_4^0$, and $Li_4SnSe_4^0$ and ideal meta-stable structures $Li_4GeS_4^*$, $Li_4SnS_4^*$, and $Li_4SnSe_4^*$. The meta-stable structures differ from the ground state configurations by the removal of the a site Li's to the so-called c' sites and the contraction of the a axis lattice parameter by approximately 0.5 Å. The ground state structures have been experimentally reported for $Li_4GeS_4^0$, $Li_4SnS_4^0$, and $Li_4SnSe_4^0$ in References 4, 4, and 5, respectively. Our ideal meta-stable structure is consistent with the structure of $Li_4SnS_4^*$ reported by Reference 3 and corroborated by References 6 and 7.

Based on these ideal structures, Li ion migration processes were computationally examined for $Li_4SnS_4^0$, $Li_4SnS_4^*$, $Li_4SnSe_4^0$, and $Li_4SnSe_4^*$. Considering simple defects and NEB analysis, we find interstitialcy mechanisms in all of these materials to provide efficient motion of the Li ions primarily along the b and c lattice directions. The small "formation energy" involved with moving a Li ion from a host lattice site into an interstitial site resulting in a interstitial-vacancy pair, $E_f = 0.15$ eV for both $Li_4SnS_4^*$ and $Li_4SnSe_4^*$ implies that these structures are likely to be disordered at relatively low temperatures as suggested by the original analysis of Kaib, Haddadpour, et al.[3] The

simulations indicate that the corresponding formation energy is larger for the ground state structures, where $E_f = 0.27$ eV for $Li_4SnS_4^0$ and $E_f = 0.36$ eV for $Li_4SnSe_4^0$, suggesting that these structures are likely to remain ordered at relatively low temperatures. At the present time, experimental measurements of the activation energy for ion conductivity are available only for $Li_4SnSe_4^0$ and $Li_4SnS_4^*$. As shown in Table VI, the NEB estimate of E_A^{NEB} for $Li_4SnSe_4^0$ is in reasonable agreement with experiment assuming an interstitialcy mechanism. On the other hand, the NEB estimate of E_A^{NEB} for $Li_4SnS_4^*$ is not in good agreement with experiment, presumably because significant contributions from more complicated configurations than the pure interstitialcy mechanism are important of ion migration in this case. Molecular dynamics simulations performed at temperatures of $T = 600K$ and higher indicate that there is significant motion of all of the Li ions including appreciable occupancy of the interstitial sites for all of the structures. Plots of the site occupancy parameters from the molecular dynamics simulations shown in Fig. 10 are consistent with the notion that the ground state structures remain more ordered for a larger temperature range than do the meta-stable structures. Sequences of the molecular dynamics steps identify the interstitialcy mechanism as well as more complicated motions which contribute to the Li ion mobility. While these molecular dynamics studies, provide interesting insight into the properties of these materials, further work is needed to reconcile the calculated tracer diffusion simulations to quantitative estimates of the ion conductivity as shown in Fig. 11. In principle if the numerical accuracy and physical approximations could be improved, it would be reasonable to attribute the difference between the tracer diffusion simulations and the conductivity measurements to the Haven ratio. However, the error bars of the present work are too large to make this connection at the present time.

The simulations suggest that both Li_4SnS_4 and Li_4SnSe_4 have two ideal phases. The current literature suggests that the ground state structure is accessible by higher temperature processing while the meta-stable structure is formed at lower temperatures. For $Li_4SnS_4^0$, MacNeil et al.[4] report their highest synthesis temperature as 1023 K, while for $Li_4SnS_4^*$, Sahu et al.[6] report the highest synthesis temperature as 723 K. Understanding how to control the physical realization of these two phases, and possibly observing the phase transition might be of interest for future investigations.

Acknowledgment

This work was supported by NSF grant DMR-1507942. Computations were performed on the Wake Forest University DEAC cluster, a centrally managed resource with support provided in part by the University. Helpful discussions with Jennifer A. Aitken from Duquesne University, Joseph H. MacNeil from Chatham University, Larry E. Rush, Jr. from Wake Forest University, and Kanchan Sarkar and Renata Wentzcovitch from the University of Minnesota are gratefully acknowledged.

References

1. Y. Wang, W. D. Richards, S. P. Ong, L. J. Miara, J. C. Kim, Y. Mo, and G. Ceder, *Nature Materials*, **14**, 1026 (2015).
2. J. Li, C. Ma, M. Chi, C. Liang, and N. J. Dudney, *Advanced Energy Materials*, **5**, 1401408 (2015).
3. T. Kaib, S. Haddadpour, M. Kapitein, P. Bron, C. Schrder, H. Eckert, B. Roling, and S. Dehnen, *Chemistry of Materials*, **24**, 2211 (2012).
4. J. H. MacNeil, D. M. Massi, J.-H. Zhang, K. A. Rosmus, C. D. Brunetta, T. A. Gentile, and J. A. Aitken, *Journal of Alloys and Compounds* (2013).
5. T. Kaib, P. Bron, S. Haddadpour, L. Mayrhofer, L. Pastewka, T. T. Jrvi, M. Moseler, B. Roling, and S. Dehnen, *Chemistry of Materials*, **25**, 2961 (2013).
6. G. Sahu, Z. Lin, J. Li, Z. Liu, N. Dudney, and C. Liang, *Energy Environ. Sci.*, **7**, 1053 (2014).
7. K. H. Park, D. Y. Oh, Y. E. Choi, Y. J. Nam, L. Han, J.-Y. Kim, H. Xin, F. Lin, S. M. Oh, and Y. S. Jung, *Advanced Materials*, **28**, 1874 (2016).
8. P. Hohenberg and W. Kohn, *Physical Review*, **136**, B864 (1964).
9. W. Kohn and L. J. Sham, *Physical Review*, **140**, A1133 (1965).
10. P. E. Blöchl, *Phys. Rev. B*, **50**, 17953 (1994).
11. N. A. W. Holzwarth, A. R. Tackett, and G. E. Matthews, *Computer Physics Communications*, **135**, 329 (2001), available from the website http://pwpaw.wfu.edu.
12. P. Giannozzi, S. Baroni, N. Bonini, M. Calandra, R. Car, C. Cavazzoni, D. Ceresoli, G. L. Chiarotti, M. Cococcioni, I. Dabo, A. D. Corso, S. de Gironcoli, S. Fabris, G. Fratesi, R. Gebauer, U. Gerstmann, C. Gougoussis, A. Kokalj, M. Lazzeri, L. Martin-Samos, N. Marzari, F. Mauri, R. Mazzarello, S. Paolini, A. Pasquarello, L. Paulatto, C. Sbraccia, S. Scandolo, G. Sclauzero, A. P. Seitsonen, A. Smogunov, P. Umari, and R. M. Wentzcovitch, *J. Phys.: Condens. Matter*, **21**, 394402 (19pp) (2009), available from the website http://www.quantum-espresso.org.
13. X. Gonze, B. Amadon, P. M. Anglade, J. M. Beuken, F. Bottin, P. Boulanger, F. Bruneval, D. Caliste, R. Caracas, M. Cote, T. Deutsch, L. Genovese, P. Ghosez, M. Giantomassi, S. Goedecker, D. R. Hamann, P. Hermet, F. Jollet, G. Jomard, S. Leroux, M. Mancini, S. Mazevet, M. J. T. Oliveira, G. Onida, Y. Pouillon, T. Rangel, G. M. Rignanese, D. Sangalli, R. Shaltaf, M. Torrent, M. J. Verstraete, G. Zerah, and J. W. Zwanziger, *Computer Physics Communications*, **180**, 2582 (2009), code is available at the website http://www.abinit.org.
14. A. Kokalj, *Journal of Molecular Graphics and Modelling*, **17**, 176 (1999), code available at the website http://www.xcrysden.org.
15. A. Kokalj, *Computational Materials Science*, **28**, 155 (2003).
16. K. Momma and F. Izumi, *Applied Crystallography*, **44**, 1272 (2011), code available from the website http://jp-minerals.org/vesta/en/.
17. J. P. Perdew and Y. Wang, *Phys. Rev. B*, **45**, 13244 (1992).
18. Y. A. Du and N. A. W. Holzwarth, *Phys. Rev. B*, **76**, 174302 (14 pp) (2007).
19. Y. A. Du and N. A. W. Holzwarth, *Phys. Rev. B*, **81**, 184106 (15pp) (2010).
20. Z. D. Hood, C. Kates, M. Kirkham, S. Adhikari, C. Liang, and N. A. W. Holzwarth, *Solid State Ionics*, **284**, 61 (2015).
21. N. D. Lepley, N. A. W. Holzwarth, and Y. A. Du, *Phys. Rev. B*, **88**, 104103 (11 pp) (2013).
22. H. Jónsson, G. Mills, and K. W. Jacobsen, in *Classical and Quantum Dynamics in Condensed Phase Simulations*, edited by B. J. Berne, G. Ciccotti, and D. F. Coker (World Scientific, Singapore, 1998) pp. 385.
23. G. Henkelman, B. P. Uberuaga, and H. Jónsson, *J. Chem. Phys.*, **113**, 9901 (2000).
24. G. Henkelman and H. Jónsson, *J. Chem. Phys.*, **113**, 9978 (2000).
25. T. Hahn, ed., *International Tables for Crystallography, Volume A: Space-group symmetry, Fifth revised edition* (Kluwer, 2002) ISBN 0-7923-6590-9. The symmetry labels used in this work are all based on this reference.
26. "Mercury 3.5.1", (2014), developed and distributed by the Cambridge Crystallographic Data Centre http://www.ccdc.cam.ac.uk/mercury/.
27. A. Al-Qawasmeh and N. A. W. Holzwarth, *Journal of the Electrochemical Society*, **163**, A2079 (2016).
28. D. R. Lide, ed., *CRC Handbook of Chemistry and Physics, 90th Edition* (CRC Press, Taylor & Francis Group, 2009) ISBN 13: 978-1-4200-9084-0.
29. S. J. Rettig and J. Trotter, *Acta Cryst. C*, **43**, 2260 (1987).
30. R. Keller, W. B. Holzapfel, and H. Schulz, *Physical Review B*, **16**, 4404 (1977).
31. J. A. Brant, D. M. Massi, N. A. W. Holzwarth, J. H. MacNeil, A. P. Douvalis, T. Bakas, S. W. Martin, M. D. Gross, and J. A. Aitken, *Chemistry of Materials*, **27**, 189 (2015).
32. Y. Mo, S. P. Ong, and G. Ceder, *Chemistry of Materials*, **24**, 15 (2012).
33. S. P. Ong, Y. Mo, W. D. Richards, L. Miara, H. S. Lee, and G. Ceder, *Energy & Environmental Science*, **6**, 148 (2013).
34. Z. Zhu, I.-H. Chu, Z. Deng, and S. P. Ong, *Chemistry of Materials*, **27**, 8318 (2015).
35. Y. Deng, C. Eames, J.-N. Chotard, F. Lalre, V. Seznec, S. Emge, O. Pecher, C. P. Grey, C. Masquelier, and M. S. Islam, *Journal of the American Chemical Society*, **137**, 9136 (2015).
36. J. M. Haile, *Molecular Dynamics Simulations* (John Wiley & Sons, Inc., 1992).
37. G. E. Murch, *Philosophical Magazine A*, **45**, 685 (1982).
38. G. E. Murch, *Solid State Ionics*, **7**, 177 (1982).
39. G. E. Murch, *J. Phys. Chem. Solids*, **46**, 53 (1985).
40. J. Maier, *Physical Chemistry of Ionic Materials* (John Wiley & Sons, Ltd., 2004).
41. K. Compaan and Y. Haven, *Trans. Faraday Soc.*, **54**, 1498 (1958).
42. B. J. Morgan and P. A. Madden, *Physical Review Letters*, **112** (2014).